Bonding in Transition Metal−Ether Complexes: The Spectroscopy and Reactivity of the Zr Atom−Dimethyl Ether System

David B. Pedersen,* Marek Z. Zgierski, Sarah Anderson, David M. Rayner, and Benoit Simard

Steacie Institute for Molecular Sciences, National Research Council of Canada, 100 Sussex Drive, Ottawa, ON, Canada, K1A OR6

Shengang Li and Dong-Sheng Yang

Department of Chemistry, University of Kentucky, Lexington, Kentucky 40506-0055

Received: August 3, 2001; In Final Form: October 18, 2001

The reactivity and bonding of neutral Zr metal atoms with dimethyl ether have been thoroughly characterized using flow tube reactor, PFI-ZEKE, and DFT techniques. Between 275 and 371 K, these species form an association complex with the Zr bound to the ether O atom. Using a flow tube reactor, the equilibrium constant for the association reaction has been found to be $6 \pm 2 \times 10^{-14}$ cm^3 at 361 ± 10 K. From this measure the Zr−dimethyl ether bond energy is estimated to be 80 ± 2 kJ mol^{-1}. The ZEKE spectrum of the association complex is reproduced very well by DFT calculations. The calculations indicate that the Zr−dimethyl ether complex is bound by dative bonding involving donation of electron density from the highest occupied dimethyl ether orbital of a_1 symmetry to the Zr 4d orbital of σ symmetry directed along the Zr−dimethyl ether bond axis. Dative bonding interactions are much stronger than donor−acceptor bonding as the vacant dimethyl ether antibonding orbital lies too high in energy for back-donation of electron density from Zr to be efficient. This finding is likely a general characteristic of neutral transition metal−ether complexes. To our knowledge, these results constitute the most detailed investigation, to date, of neutral transition metal−ether bonding and reactivity.

I. Introduction

The encapsulation of metal centers within the protective confines of host molecules represents a strategy exploited by chemists and nature in synthetic and biological systems, respectively.[1−3] The inclusion of metals within a host allows them to be dissolved in solvents in which they may otherwise be insoluble. The host also provides a means of controlling the reactions occurring at the metal center by restricting access to it. The reactivity of the complexed metal naturally depends inherently on the nature of the binding to the host and can be expected to differ as the properties of the host are changed. The encapsulation of a metal atom or ion within the confines of a crown ether results in the formation of complexes with novel catalytic properties.[4,5] Studies of the metal−ether bonding interactions can be utilized to develop an understanding of the reactivity of these metal centers.

Metal−ether complexes are expected to involve electrostatic, covalent, and dative interactions. The relative contributions of these different modes of binding affects both the metal−ether bond strength and the nature of the complexes formed upon reaction of metals with ethers. For alkali ions, the metal−ether bonding is primarily electrostatic. A theoretical study of alkali ion−ether complexes has shown that trends in ligand binding energies are well-described by a simple electrostatic model.[6] Similar findings have been reported for metal−water complexes.[7] These examples show that electrostatic models work well when the bonding at the metal center does not involve significant covalent or dative interactions. For the interaction of a neutral metal atom with an ether, dative and covalent interactions are likely to be dominant. The Al−dimethyl ether complex is thought to be such a system, involving donation of the oxygen lone-pair electron density to the vacant p orbital of Al.[8] Theoretical studies suggest that the formation of the Al−dimethyl ether association complex is 5 kcal mol^{-1} (21 kJ mol^{-1}) exothermic.[9] The study also indicates that insertion of Al into the dimethyl ether C−O bond involves surmounting a modest activation energy barrier of approximately 20 kcal mol^{-1} (84 kJ mol^{-1}). Thus, both insertion and association reactions are possible, and the identity of the experimentally observed complex(es) is not clear. Accordingly, in contrast to the ionic alkali metal−ether complexes described above where electrostatic models work well, for other metal atom−ether complexes the bonding can be complicated by the involvement of significant covalent and dative interactions and the possibility of multiple reaction products. For example, previous studies of transition metal ion reactions with ethers suggest that metal−ether bonding involves at least partial covalent interaction.[10−13] The chemistry associated with these transition metal ion−ether systems is rich and includes insertion into the carbon−oxygen bond followed by a beta-hydrogen shift. Definitive experimental data regarding the mode of bonding between neutral transition metal atoms and ethers is lacking. The lack of such experiments makes it difficult to predict whether insertion products, association complexes, or dissociative insertion will result upon reaction of a neutral transition metal atom with an ether.

* To whom correspondence should be addressed. E-mail david.pedersen@nrc.ca

10.1021/jp0130158 CCC: $20.00
Published on Web 11/29/2001

Experimental measures of metal-ether bond strengths are invaluable in the understanding of metal−ether bonding. Such measures make it possible to distinguish weak metal−ether interactions, as are characteristic of van der Waals complexes, from strong ones, characteristic of covalent bonding. Furthermore, bond strengths serve as good criteria by which the accuracy of any theoretical treatment of metal−ether complexes can be evaluated. The number of actual measures of metal−ether bond strengths, however, are very few. Several alkali ion−ether bond energies have been measured using gas-phase ion techniques. Values of 93 ± 5 kJ mol^{-1} and 254 ± 13 kJ mol^{-1} have been determined for Na^+ ion complexes with dimethyl ether and 12-crown-4 ethers, respectively.[14] For Rb^+, values of 64 ± 9 kJ mol^{-1} and 95 ± 13 kJ mol^{-1} are established for complexes with dimethyl ether and 12-crown-4 ether, while 57 ± 5 kJ mol^{-1} and 86 ± 9 kJ mol^{-1} are the binding energies of the Cs^+−dimethyl ether and Cs^+−12-crown-4 ether complexes, respectively.[15] No experimental bond energies for complexes of ethers with transition metal ions are reported in the literature. Part of the reason for the lack of data may be that transition-metal ions readily insert into C−O bonds upon reaction with ethers,[10−13] thus making it difficult to determine whether an insertion complex bond energy or an association complex bond energy is being determined. As reactions with neutral transition metal atoms are typically much less likely to involve insertion,[16] gas-phase study of neutral atom reactions represents a promising alternative to the ion studies as a means of determining transition metal−ether association complex bond strengths. In this vein, the binding energy of Al atoms with dimethyl ether and diethyl ether have been determined through the measurement of equilibrium constants.[8] The bond strengths were found to be 9.2 ± 0.6 kcal mol^{-1} (38 ± 3 kJ mol^{-1}) and 9.2 ± 1.2 kcal mol^{-1} (38 ± 5 kJ mol^{-1}) for dimethyl ether and diethyl ether, respectively. Theory has successfully reproduced the Al−dimethyl ether bond energy.[9] For the Cr atom complex with the same two ethers the rate of the association was found to be very small, indicative of a bond energy smaller than that of the Al complexes.[17]

To better characterize the bonding in metal−ether complexes, measurements of metal−ether bond energies can be complemented with spectroscopic characterization of the reaction product. Spectroscopy provides a means by which the elimination, association, and insertion reaction channels possible in metal atom−ether reactions can be distinguished. Of the many spectroscopic techniques available, pulsed-field ionization, zero kinetic energy electron (PFI-ZEKE) spectroscopy has the advantage that transitions between the electronic ground states of the neutral and of the cation can be probed.[18] As the ground state of the ion is probed, a minimal amount of energy is available for intramolecular processes and the probability of photoinduced dissociation is minimal, accordingly. ZEKE therefore provides a means of spectroscopically probing weakly bound complexes that may dissociate using other techniques.

To contribute to the general understanding of transition metal−ether bonding and reactivity, the nature of the complex formed during the gas-phase reaction of neutral Zr atoms with dimethyl ether is the topic of this paper. Preliminary results have already been published.[19] Using flow tube techniques, an equilibrium constant for the Zr−dimethyl ether association reaction has been determined from which the bond energy of the complex has been estimated to be 80 ± 2 kJ mol^{-1}. The complex has also been interrogated using PFI-ZEKE spectroscopy. For the ground states of both neutral and cationic species, an association complex geometry with the Zr atom positioned adjacent to the ether O atom (C_{2v} symmetry) is found to be most consistent with the spectrum observed. Using the ZEKE spectrum as a criterion, density functional theory (DFT) is found to provide a good description of the Zr−dimethyl ether and Zr−dimethyl ether$^+$ systems. Based on this good agreement, the nature of Zr−ether bonding in the neutral species has been analyzed using the theory. The bonding is found to be primarily a dative bond involving donation of electron density from dimethyl ether to Zr. Within the context of molecular orbital theory, this bonding occurs primarily through favorable interactions between the highest occupied dimethyl ether orbital of a_1 symmetry and the Zr 4d orbital of σ symmetry directed along the Zr−dimethyl ether bond axis. To our knowledge, this study is the most detailed investigation of a neutral transition metal−ether complex to date and as such constitutes a benchmark for calibration of theoretical treatments of such systems.

II. Experimental Methods

A. ZEKE Experiment. The molecular beam ZEKE apparatus has been described previously.[18] It consists of two vacuum chambers. The first chamber houses a Smalley-type laser ablation supersonic expansion source[20] and is pumped by a 2200 L s^{-1} oil diffusion pump. The second chamber houses the ZEKE spectrometer and is pumped by two 400 L s^{-1} turbomolecular pumps. The spectrometer consists of a two-stage extraction assembly, a 34 cm long flight tube, and a dual microchannel plate detector, and is encased in a cylindrical, double-walled, μ-metal shield. The spectrometer could also be operated as a two-field, space-focused, Wiley−McLaren[21] time-of-flight mass spectrometer by supplying appropriate voltages. Zirconium atoms were produced by Nd:YAG laser vaporization (532 nm, 1.5 mJ pulse^{-1}, 6 ns, focused by a 30 cm focal length lens) of a zirconium rod (Goodfellow, > 99.8%) in the presence of a pulse of helium gas (2 atm stagnation pressure). The zirconium atoms reacted with dimethyl ether (Matheson, 99.8%) seeded in the helium gas with a concentration of 5 × 10^{-1}%. The resultant molecular beam passed down a liquid nitrogen cooled tube (2 mm inner diameter, 2 cm length) and was supersonically expanded into the vacuum chamber. The supersonic jet was skimmed 5 cm downstream from the exit end of the tube. A deflection field was applied to remove residual charged species in the molecular beam before it entered the second chamber. Prior to the ZEKE experiments on Zr−dimethyl ether, single-photon photoionization efficiency curves were measured to locate the approximate ionization potential of the molecule. Time-of-flight mass spectrometric measurements were taken to optimize the experimental conditions such that the ratio of the Zr−dimethyl ether signal in the mass spectrum to that of any other species was maximized. With the optimized conditions, Zr−dimethyl ether was excited to high-lying Rydberg states by a single-photon process. The high-lying Rydberg states were then ionized by a delayed voltage pulse (3 μs delay, 1.0 V cm^{-1}, 100 ns width). The collection of the ZEKE electrons as a function of the excitation photon wavelengths produced the high-resolution ZEKE spectrum. All of the experiments were conducted at the NRC, Ottawa.

B. Flow Tube Reactor Experiments. The flow tube apparatus has also been described previously.[22−24] Zr atoms were generated using a Smalley-type laser ablation source. A pulsed XeCl laser focused onto a translating and rotating Zr metal rod, over which a 15000 sccm (standard cm^3 min^{-1}) continuous flow of He (99.995% pure from Liquid Carbonics Inc.) was maintained, generated a metallic plasma entrained in the He flow. The He-plasma gas passed through a 1 cm-long channel 0.2

cm in diameter and subsequently expanded into a large-bore (7.3 cm in diameter) flow tube reactor. The bath gas pressure in the flow tube was varied between 0.5 and 6 Torr by partially closing the gate valve to the vacuum (600 L s^{-1} Edwards EH2600 Roots blower backed by an Edwards E1M275 mechanical pump). Dimethyl ether (Matheson, 99.8%) was introduced through a shower head inlet 60.6 cm downstream from the cluster source. Reagent gas pressure in the reactor was controlled by a mass flow controller (MKS model 1159). The bath gas temperature was varied by changing the temperature of ethylene glycol flowing through a water jacket coiled around the outside of the flow tube wall. Upon reaching the end of the flow tube, a sample of the flow tube contents was passed into the reflectron time-of-flight mass spectrometer (TOFMS) situated perpendicular to the flow tube axis. A pressure drop of approximately 6 orders of magnitude between the TOFMS and the flow tube was maintained by differential pumping using an Edwards Diffstak 2300 L s^{-1} diffusion pump and an Edwards Diffstak 800 L s^{-1} diffusion pump in conjunction with an electromagnetic shutter used to reduce gas load. Zr atoms and reaction products entering the TOFMS were photoionized by a pulsed ArF exciplex laser operating at 193 nm and triggered at a set delay with respect to the firing of the ablation laser. The detector signal was digitized and sent to a personal computer for analysis. The mass spectra collected were averaged 200 times.

Bath gas pressures above 2 Torr exceed the regime within which the low pressure, prerequisite for use of the time-of-flight mass spectrometer, can be maintained by the differential pumping system. At higher pressures it was therefore necessary to switch to fluorescence detection to monitor Zr atom depletion. The system configuration employed for fluorescence detection has been described previously.[24] In the present experiments the 298.6 nm $^3F_2 \rightarrow {}^3D_1^0$ transition of Zr was excited with a YAG pumped dye laser. The 597.3 nm output of the dye laser was then frequency doubled to give 298.6 nm. Fluorescence was detected using a photomultiplier tube equipped with a bandpass filter that prevented the excitation laser light from striking the detector. All measured rate coefficients are accurate to ±50% and precise to ±10%.[23]

C. Theory. Density functional methods were used to calculate the structures and force fields of various spin states of the neutral species and of the radical cations. The B3P86 exchange-correlation functional[25,26] was used together with the LANL2DZ basis set.[27] The calculations were performed using the Gaussian suite of programs.[28]

III. Results and Discussion

In combination, the flow-tube and PFI-ZEKE results provide a thorough characterization of the neutral Zr-dimethyl ether complex. It will be shown that in both flow-tube and ZEKE experiments, Zr−dimethyl ether forms an association complex. Both the bond energy and spectrum of this complex are determined. An analysis of the spectrum reveals that the geometries of the ground electronic states of the neutral and cationic Zr−dimethyl ether complexes are very similar. These results are reproduced by DFT calculations. Based on the good agreement between theory and experiment, the DFT results are used to analyze the bonding involved in the Zr−dimethyl ether system. The bonding will be shown to be primarily dative with donation of electron density from dimethyl ether to the Zr $4d_\sigma$ orbital.

A. The Zr-Dimethyl Ether Association Reaction. *1. Kinetic Analysis.* Zr atom depletion was observed between 275 and 371 K at bath gas pressures ranging from 1 to 6 Torr. The depletion kinetics are characteristic of a reversible association reaction:

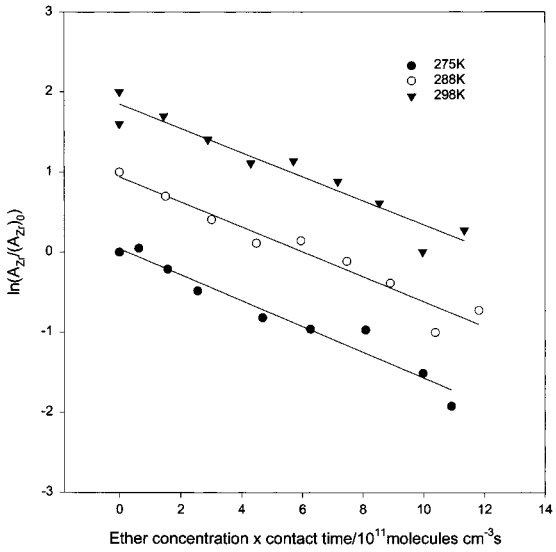

Figure 1. Pseudo first-order kinetic plots for the depletion of Zr atoms by dimethyl ether are shown for temperatures of 275, 288, and 298 K. The flow-tube pressure was 1 Torr for all of the data shown. The solid lines are fits of a pseudo first-order kinetics expression to the data as discussed in the text. The 288 and 298 K data are offset vertically by 1 and 2 units, respectively.

$$\mathrm{Zr} + \mathrm{H_3COCH_3} \xrightarrow{k_1 p(L)} \mathrm{ZrO(CH_3)_2} \quad (1)$$

$$\mathrm{ZrO(CH_3)_2} \xrightarrow{k_{-1}} \mathrm{Zr} + \mathrm{H_3COCH_3} \quad (2)$$

for which the expression

$$[\mathrm{Zr}] = \frac{[\mathrm{Zr}]_0}{1 + K \times p(L)} \times (1 + K \times p(L)\, \mathrm{e}^{-(k_1 p(L) + k_{-1})\tau}) \quad (3)$$

provides a complete description of the flow tube reactor yields.[29] Here, $p(L)$ is the partial pressure of dimethyl ether, K is the equilibrium constant for the association reaction ($K = k_1/k_{-1}$), and τ is the Zr atom−dimethyl ether contact time in the flow tube reactor.

For an association reaction, the rate of complex dissociation, k_{-1}, is intrinsically dependent on the reaction temperature. At lower temperatures where k_{-1} is relatively small, eq 3 reduces to[30]

$$\ln\frac{[\mathrm{Zr}]}{[\mathrm{Zr}]_0} = -k_1 p(L)\tau \quad (4)$$

which is a pseudo first-order expression for depletion of Zr atoms. At the lower temperatures investigated, plots of ln([Zr]/[Zr]$_0$) versus $p(L)\tau$ were found to be linear, as seen in Figure 1. In Figure 1 (as well as Figure 2 and Figure 3 below) A_{Zr} denotes signal peak area which is proportional to [Zr]. The effective rate coefficients extracted from the slopes of these plots, k_{obs}, are shown in Table 1. A slight dependence of these rate coefficients on temperature, evident in Table 1, is attributed to violation of the assumption of small k_{-1} used to derive eq 4. This observation is consistent with the onset of equilibrium occurring at higher temperatures. Similarly, at higher temperatures, deviations of plots of ln([Zr]/[Zr]$_0$) vs $p(L)\tau$ from linearity clearly signal the onset of equilibrium. An illustration of the type of deviation observed at higher temperatures is shown in

TABLE 1: Pseudo First-Order Rate Coefficients (k_{obs}) for the Removal of Zr by Dimethyl Ether

temperature/K	rate coefficient/10^{-12} cm^3 s^{-1}
275	2.38
288	1.87
298	1.16

[a] Rate coefficients are accurate to ±50% and precise to ±10% (see text).

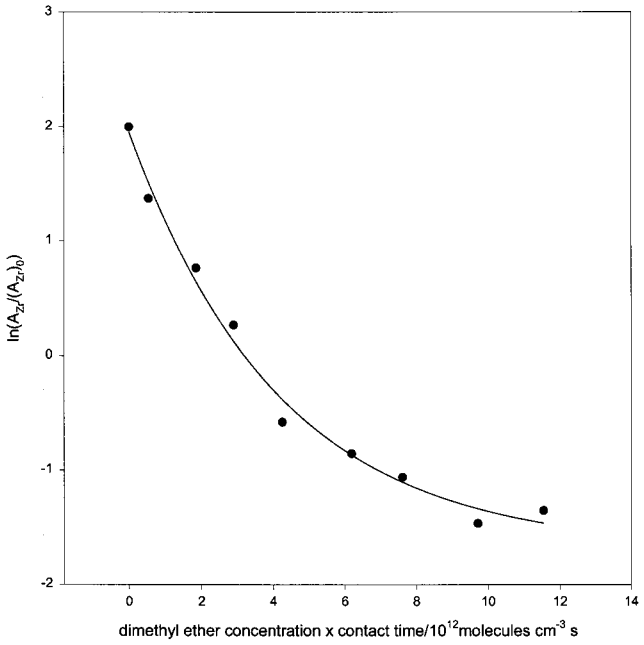

Figure 2. Pseudo first-order kinetics plot for the depletion of Zr atoms by dimethyl ether at 371 K, 4 Torr. The solid line is drawn as a guide to the eye.

Figure 2. As the magnitude of k_{-1} increases at higher temperatures, the effects of the dissociation reaction, $ZrO(CH_3)_2 \rightarrow Zr + H_3COCH_3$, on the rate of Zr atom depletion observed become increasingly significant, leading to curvature in the pseudo first-order kinetics plots. Under these conditions, the full kinetics expression, eq 3, must be employed to interpret the data.

Using both k_1 and K as variables, eq 3 has been fit to the 351, 361, and 371 K data—the temperatures at which pseudo first-order kinetics plots are curved. A sample fit is shown as a solid line in Figure 3. Agreement with the experimental data is reasonable. At lower pressures, these fits are found to be very sensitive to the value of k_1 used but not to the value of K. At higher pressures, the reverse is true. This behavior is predicted by eq 3. When τ is relatively large, as is the case in the flow tube reactor when flow tube pressure is high, the $K \times p(L)$ $e^{-(k_1 p(L)+k_{-1})\tau}$ term in eq 3 becomes negligible and only K has an effect on the kinetics. The high-pressure data therefore provide the best estimate of K. Accordingly, the high-pressure data have been used to determine a value of K. Similarly, a value of k_1 has been determined using the low-pressure data. Values of $9 \pm 5 \times 10^{-13}$ cm^3 s^{-1} and $6 \pm 2 \times 10^{-14}$ cm^3 are found for k_1 and K, respectively, in the 351 to 371 K temperature range.

The $9 \pm 5 \times 10^{-13}$ cm^3 s^{-1} value of k_1 is small for a metal atom association reaction lacking an activation energy barrier. Analogous reactions of Zr atoms with alkenes, where barrierless association complex formation is thought to be rate-determining, are $55 \pm 16 \times 10^{-12}$ cm^3 s^{-1}, and $135 \pm 40 \times 10^{-12}$ cm^3 s^{-1} for ethene and propene, respectively.[31] The comparatively small

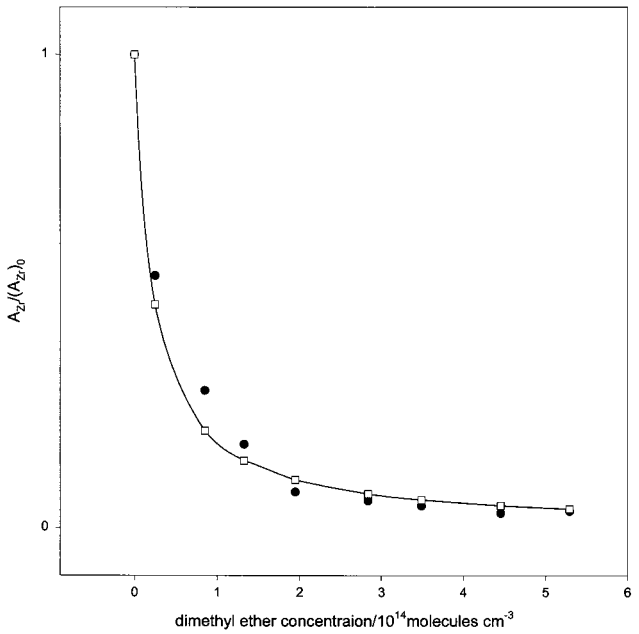

Figure 3. Kinetics plot for the association reaction of Zr with dimethyl ether. The solid points are data collected at 371 K, 4 Torr. The open points were generated by fitting the full kinetics expression for an association reaction to the data, as discussed in the text. The line is a guide to the eye.

value of k_1 for Zr−dimethyl ether may be attributable to the pressure dependence of k_1. For the Al−dimethyl ether association reaction, the high-pressure limit of k_1 lies above 600 Torr (8×10^4 Pa). By comparison, for the 1 to 6 Torr range examined in our Zr−dimethyl ether experiments, k_1 is likely in the low-pressure regime. In this case, a larger value of k_1 is expected at higher pressures. At this time we are unable to perform experiments in this regime with the flow tube apparatus, so the pressure-dependence of k_1 was not investigated further.

2. The Zr−Dimethyl Ether Bond Strength. To help characterize the metal−ether bond, an estimate of the Zr−dimethyl ether bond strength can be made from the equilibrium constant. From above, values of K could be determined only over the 351 to 371 K range and were equivalent within error. Without knowledge of the temperature dependence of K, a van't Hoff plot cannot be constructed and we use a third law analysis. From statistical mechanics

$$K = \frac{Q_{\mathrm{ZrDME}}}{Q_{\mathrm{Zr}} Q_{\mathrm{DME}}} \times e^{-E_0/kT} \qquad (5)$$

where Q_{ZrDME} and Q_{Zr}, Q_{DME} are the partition functions for the complex and reagents, respectively, k is Boltzmann's constant, and E_0 is the energy difference between the zero point energies of the free reagents and the complex. For this third law analysis, each partition function is assumed to consist of only translational, rotational, and vibrational components. That is, the electronic contribution is ignored. Calculation of the translational partition function is straightforward. The rotational component is determined by calculating the moments of inertia of dimethyl ether and the Zr−dimethyl ether complex using the geometry of the complex shown in Figure 4 and the UNIMOL program.[32] The geometry was determined using DFT, the results of which are described in more detail below. The moment of inertia values calculated are shown in Table 2. All internal rotors are assumed to be the same in both the complex and the free reagents. The vibrational partition functions were calculated using frequencies

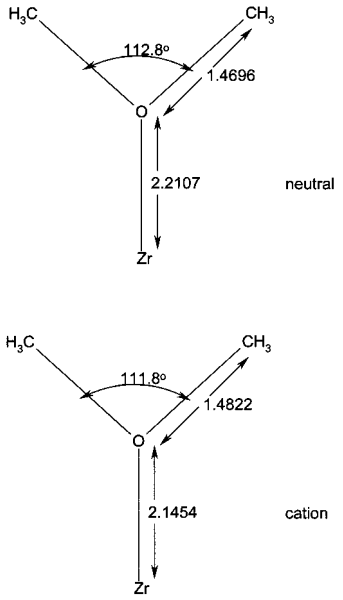

Figure 4. Geometry of the neutral Zr−dimethyl ether complex used in the second law analysis. The lower figure is a sketch of the geometry of the Zr−dimethyl ether cation predicted by DFT. See text for details.

TABLE 2: Moments of Inertia along the Three Principal Axes (A, B, C) Used to Calculate the Rotational Partition Functions of Dimethyl Ether and the Zr−Dimethyl Ether Association Complex (units are Å² amu)

molecule	A	B	C
dimethyl ether	66	60	12.3
Zr-dimethyl ether	293	239	60

TABLE 3: Vibrational Frequencies of Zr−Dimethyl Ether Complex as Determined by DFT and PFI-ZEKE (units are cm^{-1})

	expt cation	neutral	DFT cation	DFT neutral
Zr−O stretch	254	214	263	240
COC bend	450	413[a]	464	439
C−O stretch	856	919[a]	844	859
OCH_3 out of plane deformation	not observed	not observed	247	288
COZr deformation	not observed	not observed	176	167
CH_3 torsion	not observed	not observed	125	152

[a] Free $(CH_3)_2O$ IR measurement.

calculated by DFT (see below). The wavenumber values assumed for these modes are shown in Table 3. Frequencies not tabulated are effectively equivalent in both the Zr−dimethyl ether complex and the free ether. Substitution of these values for the partition functions and the $6 \pm 2 \times 10^{-14}$ cm^3 value of K into eq 5 yields an E_0 value of 80 ± 2 kJ mol^{-1}.

DFT calculations predict that Zr and dimethyl ether form a stable association complex, in agreement with the flow-tube results. The theory also predicts a spectrum in good agreement with the PFI-ZEKE spectrum (see below). However, a Zr−dimethyl ether bond energy could not be determined. At the B3P86/LANL2DZ level of theory the ^{5}F electronic configuration is predicted to be the ground state of the Zr atom. Experimentally, the ^{3}F configuration has been established as the ground state.[33] The correct ordering of the triplet and quintet states can be obtained only by high level ab initio calculations. For example, the QCISD/DZVP method[34,35] places the triplet state 0.33 eV (32 kJ mol^{-1}) below the quintet. If it is assumed that the ^{5}F state of Zr is artificially depressed in energy by the DFT and that the energy of the ^{3}F state is approximately correct,

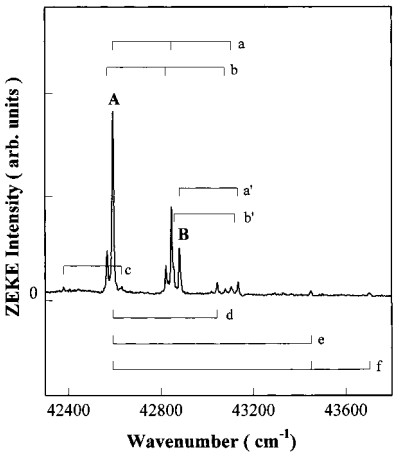

Figure 5. PFI-ZEKE spectrum of Zr−dimethyl ether. Labeled transitions are discussed in the text.

then the difference between the energy of the ^{3}F + dimethyl ether reagents and the energy of the bound complex, that is, the binding energy, is 1.15 eV (111 kJ mol^{-1}). This value agrees with the 80 ± 2 kJ mol^{-1} found from the equilibrium constant above, within the 20 to 40 kJ mol^{-1} error expected of such DFT calculations. However, failure to predict the relative energies of the separated Zr + dimethyl ether reagents precludes the determination of the Zr-dimethyl ether binding energy using the DFT method. The fact that the theory predicts properties of the Zr−dimethyl ether *complex* in good agreement with experiment (see below) suggests that problems with the theory do lie near the asymptotes (separated reagents) and not near the minima of the potential energy wells associated with Zr−dimethyl ether.

B. Spectroscopy of the Zr−Dimethyl Ether Association Complex. The PFI-ZEKE spectrum of Zr−dimethyl ether recorded at 100 K is shown in Figure 5. The spectral bandwidth at half-maximum is 6 cm^{-1}. The first ionization potential, as measured from the position of the most intense peak (A), is 5.281(1) eV (509.5 kJ mol^{-1}). The spectrum consists of a number of short progressions or energy intervals. These intervals are 254 cm^{-1} in the cases of a, b, c, a′, and b′; 450 cm^{-1} in d; 856 cm^{-1} in e; and 287 cm^{-1} between the bands A and B (see Figure 5). In addition, the progression f is the combination of the 856 cm^{-1}and 254 cm^{-1} bands. The transitions labeled b, c, and b′ are hot bands as their intensities, relative to the other band intensities, depended on the conditions of the molecular beam source.

An initial spectral assignment can be made by comparing the ZEKE spectrum of the complex with the infrared and Raman spectra of dimethyl ether. In free dimethyl ether, two symmetric modes, C−O−C bend and C−O stretch, have vibrational wavenumbers (413 cm^{-1}and 929 cm^{-1}) comparable to those measured in the d and e intervals.[36] The similar magnitudes of the 413 and 929 cm^{-1} dimethyl ether values and the 450 and 856 cm^{-1} Zr−dimethyl ether values suggest that the latter correspond to COC bending and C−O stretching modes in the cationic Zr−dimethyl ether complex. The appearance of bands associated with these modes indicates that the spectrum corresponds to a Zr-dimethyl ether complex in which the COC framework is intact. This result is consistent with the molecule being an association complex as suggested by the flow-tube results. Also by comparison, the Zr−dimethyl ether modes associated with the 287 and 254 cm^{-1} values are likely attributable to vibrations involving motion of Zr^+ or electronic transitions associated with the metal ion, as no other symmetric modes in free dimethyl ether are below 400 cm^{-1}.

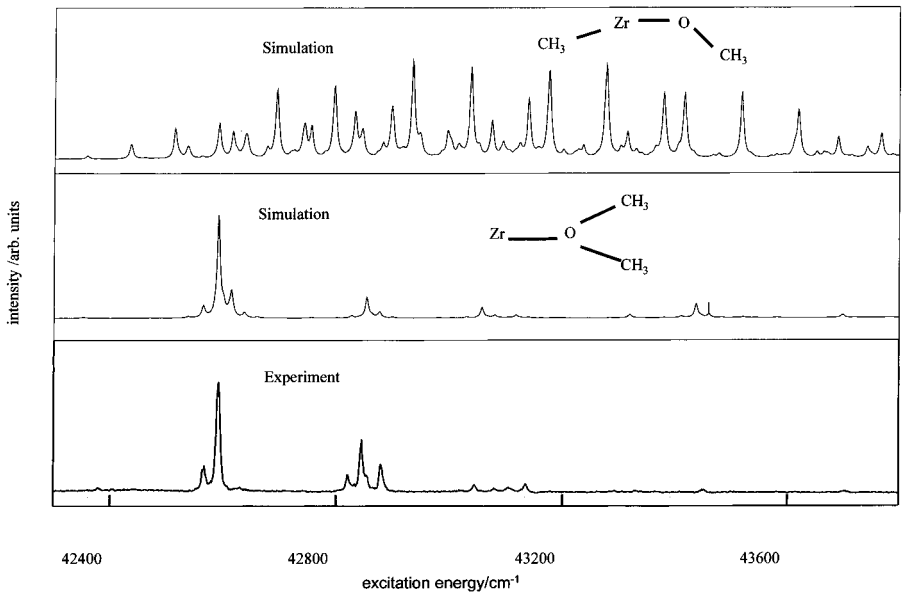

Figure 6. Comparison of the experimental (bottom) and theoretically determined spectra of Zr−dimethyl ether. Simulated spectra (100 K) for association (C_{2v}) (middle) and insertion (top) geometries of Zr−dimethyl ether are shown. The theoretical spectra have been shifted so that the origins of the spectra coincide with the origins of the experimental spectra.

To facilitate assignment of the PFI-ZEKE spectrum, DFT calculations of the properties of neutral and cation Zr−dimethyl ether complexes were performed. Stable geometries for both insertion and association-type complexes, both neutral and cationic, were found. For the neutral, an association complex of C_{2v} symmetry with the Zr bonded to the O atom was found to be the most likely reaction product. No significant energy barrier is predicted to impede the formation of this product. An insertion complex, with Zr inserted in one of the C−O bonds, lies lower in energy but is separated from the ground state of the Zr−dimethyl ether association complex by an energy barrier. The neutral association complex geometry is shown in Figure 4. The complex is a triplet of B_1 symmetry. The C_{2v} geometry was also predicted to be stable for the cation. As seen in Figure 4 the neutral and cation C_{2v} species have very similar geometries with a small change in the Zr−O bond length being the only significant difference. In accord with the Franck−Condon principle, electronic transitions between these two species should therefore manifest only a short progression, due to the similar geometries, consistent with the spectrum observed, Figure 5.

To simulate the spectrum, we performed DFT (B3P86/LANL2DZ) vibrational analysis and Franck−Condon calculations. Franck−Condon intensities were calculated using the DFT geometries, harmonic vibrational wavenumbers, and force field. Three symmetric modes are predicted to be active: Zr^+−O stretch (263 cm^{-1}), C−O−C bend (464 cm^{-1}), and C−O stretch (844 cm^{-1}). All other symmetric modes are greater than 1200 cm^{-1} and are predicted to have little Franck−Condon activity. The theoretically predicted spectrum of transitions between the ground electronic states of the C_{2v} neutral and cation species is shown in Figure 6 (middle). The origin of the theoretical spectrum has been shifted by 2060 cm^{-1} (24 kJ mol^{-1}) so that the origins of the predicted and ZEKE spectra are coincident in energy. This shift compensates for error in the calculation, which predicts an ionization energy of 5.54 eV (530 kJ mol^{-1}) compared with the 5.281(1) eV (509.5 kJ mol^{-1}) experimental value, as defined by the origin of the ZEKE spectrum, Figure 5. This error is within the 5 kcal mol^{-1} to 10 kcal mol^{-1} (20 kJ mol^{-1}-40 kJ mol^{-1}) range typically cited for DFT calculations of this type. As seen in Figure 6, the theoretical and experimental spectra agree very well. Also shown in Figure 6 (top) is the theoretically predicted spectrum for transitions between the ground states of neutral and cationic Zr−dimethyl ether of an insertion-type geometry. In this complex the Zr has inserted into one of the dimethyl ether C−O bonds. This geometry is also predicted to be stable for both neutral and cationic species. However, as seen in Figure 6, transitions between these species are predicted to manifest a spectrum of long progressions. The poor match between this spectrum and that observed indicates that the insertion complex is not responsible for the spectrum observed. Based on the sharp contrast in the forms of the predicted spectra, the DFT calculations indicate that a Zr−dimethyl ether association complex of C_{2v} symmetry is responsible for the observed spectrum. The experimentally observed spectral transition energies and the energies of the normal modes of the C_{2v} cation and neutral species, as predicted by DFT, are shown in Table 3. In general, good agreement between theory and experiment is observed. Based on this agreement the experimentally observed bands have been assigned, as shown in Table 3.

The theoretical wavenumber of the Zr^+−O stretch (263 cm^{-1}) is close to the experimental value of 254 cm^{-1}, but also not very far from the value of 287 cm^{-1}. This implies that either of the measured 254 or 287 cm^{-1} intervals could be attributed to the Zr^+−O stretch. However, in the ZEKE spectrum shown in Figure 5, the 254 cm^{-1} interval forms well-structured vibrational patterns, such as a, b, and f, while little pattern is seen with the 287 cm^{-1} interval. The formation of patterns of familiar structure suggests that 254 cm^{-1} corresponds to the Zr^+−O stretch. Furthermore, if the 287 cm^{-1} interval were assigned to the Zr^+−O vibration, most spectral features, such as a, b, f, a′, and b′, would be difficult to explain. With the 254 cm^{-1} interval being assigned to the Zr^+−O mode, a wavenumber of 214 cm^{-1} measured from the hot bands labeled c can be attributed to the Zr−O stretch in the neutral complex. The experimental value of 214 cm^{-1} is in fair agreement with the theoretical wavenumber of 240 cm^{-1} for this neutral stretch mode. In addition, the hot bands labeled b and b′ are 25 cm^{-1} to the red of the corresponding members of the cold bands a and a′. This observation indicates that there exists a vibrational mode, 25 cm^{-1} larger in the neutral than in the ion complex. From our DFT calculations the CH_3 torsion (a_2) is predicted to be 152

cm^{-1} in $Zr-O(CH_3)_2$ and 125 cm^{-1} in $Zr^+-O(CH_3)_2$. The theoretical difference of 27 cm^{-1} matches well with the measured difference of 25 cm^{-1}.

The band B, 287 cm^{-1} to the blue of the band A in Figure 5, may be assigned to another electronic state of $Zr^+-O(CH_3)_2$. However, our DFT calculations find no other quartet state lying close to the ground state $^4B_1$ of $Zr^+-O(CH_3)_2$. A doublet, $^2B_2$, is predicted to be 0.38 eV higher than the $^4B_1$ state. This doublet is too far apart from the ground state to be responsible for the observed 287 cm^{-1} transition. Also, if the $^2B_2$ state were observed in the ZEKE spectra, a different Zr^+-O vibrational wavenumber would be expected from that of the $^4B_1$ state. However, the spectrum shows the same 254 cm^{-1} interval being superimposed on the two band origins (A and B). A third possibility for the 287 cm^{-1} transition is the spin−orbit splitting arising from the coupling of the $^4B_1$ and $^2B_2$ states. Our DFT calculations consider no spin−orbit effect, and a comparison between the experiment and theory is not possible at this point. However, theoretical treatments of such effects have been reported on other metal-containing polyatomic systems.[37,38] For example, in the case of SnH_2, calculations have predicted that the coupling of the $^1A_1$ and $^3B_1$ states ($\Delta E = 1.1$ eV) splits the $^3B_1$ state into three levels: $^3B_1(A_1)$,$^3B_1(A_2)$ and $^3B_1(B_2)$. The splitting is predicted to be 312 cm^{-1} between $^3B_1(A_1)$ and $^3B_1(A_2)$, and 4 cm^{-1}between $^3B_1(A_2)$ and $^3B_1(B_2)$. Assigning the band B to a second spin−orbit component of the $^4B_1$ state also explains the same Zr^+-O vibrational wavenumbers measured for the two spin levels. Furthermore, the 287 cm^{-1} splitting is comparable to the splitting of 315 cm^{-1} between the $^4F_{1.5}$ and $^4F_{2.5}$ levels of the ground state $^4F(4d^25s)$ of the free Zr^+.[33]

C. Bonding in the Metal−Ether Complexes. The combination of measurement of bond strength, theoretical calculation, and observed spectroscopy provides a relatively thorough characterization of the neutral Zr−dimethyl ether complex and insight into the nature of bonding in neutral transition metal−ether complexes. It is clear from both spectroscopy and theory that the neutral Zr−dimethly ether complex is an association complex in which the Zr atom is situated adjacent to the dimethyl ether O atom. The close proximity of the metal and O atoms is indicative of favorable interaction between Zr and the lone pair of electrons present on O.

Similar interactions of Zr with the π electrons of ethene have been reported, and a bond strength of 35 kcal mol^{-1} (150 kJ mol^{-1}) has been predicted.[39] The strong interaction is explained in terms of the Dewar-Chatt-Duncanson mechanism of bonding.[40,41] The model involves donation of Zr atom 4d electron density into a vacant ethene antibonding orbital and the simultaneous donation of σ electron density from ethene to a vacant Zr orbital of σ-type symmetry. In the case of dimethyl ether, although the lone pairs on the ether O are prime candidates for analogous donation to the metal in the Zr−dimethyl ether complex, our DFT shows that the vacant dimethyl ether antibonding orbital available for back-donation lies much higher in energy and back-donation is disfavored. Strong Dewar-Chatt-Duncanson-type interactions between Zr and dimethyl ether are therefore precluded by the orbital structure of the Zr−dimethyl ether system. In this context, the large difference in Zr−ethene (146 kJ mol^{-1}) and Zr−dimethyl ether (80 ± 2 kJ mol^{-1}) bond energies reflects large differences in the contribution of donor−acceptor interactions to the binding of the two complexes as a result of differences in molecular orbital structure.

A dative bond without back-donation is supported by the DFT results. The agreement between the DFT results and the experimentally determined spectrum indicates that the molecular orbital picture inherent in the DFT calculations is, for the most part, correct. Accordingly, the DFT results can be used to understand the bonding in the neutral Zr−dimethyl ether complex. A net negative charge, reflecting electron donation characteristic of dative bond formation, lies on the Zr atom in the Zr−dimethyl ether complex. There is no evidence of back-donation characteristic of strong Dewar-Chatt-Duncanson bonding. The major contributor to the bonding is the highest occupied orbital of a_1 symmetry. This orbital is a composite of the highest occupied orbital of a_1 symmetry of dimethyl ether and the Zr $4d_\sigma$ orbital, which is directed along the Zr−dimethyl ether bond axis. Dative bonding therefore occurs primarily via donation of the dimethyl ether electron density into the Zr $4d_\sigma$ orbital.

TABLE 4: M−O Bond Lengths in Transition Metal−Ether and Transition Metal−Crown Ether Complexes (units are Å)

	observed[a]	sum of atomic covalent radii
Zr−crown ether	1.93, 2.24, 2.33	2.21
Ti−crown ether	2.09, 2.15, 2.14	2.09
Hf−crown ether	2.21	2.23
Zr-dimethyl ether	2.21[b]	2.21

[a] Reference 42. [b] From DFT as described in text.

Dative bonding in the Zr-dimethyl ether complex formed in the gas phase does not preclude the formation of stronger Zr−ether bonds formed in other media or via other reaction paths. The DFT, for example, predicts stable association and insertion geometries. Solution phase Zr−crown ether complexes display evidence of stronger covalent interactions. In its crystalline form the ground-state structure of the Zr−crown ether 18-crown-6 compound, determined using crystallographic techniques, contains two distinguishable types of Zr−O (where O is part of the ether ring) bonds.[42] Four of the Zr−O bonds are relatively long with Zr−O bond lengths near 2.24 Å.[42] This bond length is comparable to that of the Zr−dimethyl ether complex, as determined by theory. The compound also contains one shorter Zr−O bond of length 1.93 Å indicative of a stronger bonding interaction. By comparison the bond length of the gas-phase diatomic ZrO, which likely involves a bond of multiple order, is 1.71 Å.[43] Within the 2.24 Å to 1.71 Å range of bond lengths observed, the 1.93 Å lies closer to the covalent 1.71 Å value, which suggests that 1.93 Å is appropriate for a strong, possibly double, Zr−O bond. The presence of such a strong Zr−crown ether covalent bond appears to be at odds with the near absence of such strong covalent interactions in the Zr−dimethyl ether complex. The formation of such a bond is certainly thermodynamically favored. For the gas-phase reaction of neutral Zr atoms with dimethyl ether, the formation of covalent bonds much stronger than the dative bonding observed is likely impeded by activation energy barriers. Such barriers are common in reactions involving neutral transition metal atoms[16,39,44−46] In the solution-phase synthesis of the Zr−crown ether complex, the ionic $ZrCl_4$ starting material employed implicates the participation of ionic Zr in the Zr−crown ether complexation reaction. For transition metal ions, the presence of charge often manifests a significant decrease in the magnitude of activation energy barriers present in the analogous neutral reaction.[16,47] Thus the formation of a strong covalent bond in the Zr−crown ether complex may arise from the involvement of Zr ions in the solution-phase synthesis of this compound.

As a model of metal−crown ether interactions, it is useful to compare the Zr−O bond length of the Zr−dimethyl ether complex with known metal−crown ether bond lengths. In crown ether complexes metal centers are typically coordinated at several O atom sites. In Table 4 the measured metal−O bond

lengths in Ti, Zr, and Hf complexes with crown ethers are shown along with the Zr−O bond length calculated for Zr−dimethly ether. For comparison, the sums of the covalent radius of oxygen with the covalent radii of the metal atoms are also listed in Table 4. As seen, there is relatively good agreement between experiment and the predicted covalent bond lengths. These results suggest that covalent bonding may be a common feature of transition metal−crown ether complexes. However, good agreement between the calculated and experimental bond lengths can also be had by assuming that bonding occurs between multiply charged metals, that is, higher oxidation states, and doubly charged oxygen anions. The observed bond lengths are therefore consistent with either covalent or ionic bonding. For Zr−dimethyl ether it is clear that the metal is not in a high oxidation state and that the bonding is not ionic. For this complex there is also good agreement between the covalent Zr−O bond length and that determined for Zr−O by DFT (see above). Based on this agreement, it is possible to associate the predicted covalent bond lengths with dative bonding interactions of the type found in the Zr−dimethyl ether complex. Accordingly, such dative interactions must be considered as potentially responsible for much of the bonding in all of the metal−ether complexes listed in Table 4.

IV. Summary and Conclusions

The nature of bonding in the Zr−dimethyl ether complex has been characterized. Both the gas-phase reaction of Zr atoms with dimethyl ether, in the 275 to 371 K and 1 to 6 Torr temperature and pressure ranges, respectively, and the PFI-ZEKE spectrum show that Zr-dimethyl ether is an association complex with the Zr bound to the oxygen atom. The bond energy of the complex is 80 ± 2 kJ mol^{-1}. DFT calculations successfully reproduce the PFI-ZEKE spectrum and establish a C_{2v} geometry for the complex. Based on the DFT results, bonding in the complex is found to occur via formation of a dative bond involving electron donation from dimethyl ether to the $4d_\sigma$ orbital of Zr. A back electron donation from Zr to the ligand is ineffective due to the relatively high energy of vacant dimethyl ether orbitals capable of accepting electron density from the Zr atom. As a general model of metal−ether bonding, if the disparity in ether acceptor and metal donor orbital energies does not change significantly for different transition metals, ineffective acceptor−donor type bonding can be expected to be a characteristic of transition metal−ether complexes. Accordingly, relatively weak dative bonds analogous to those found in the Zr−dimethyl ether system can be expected. The formation of stronger covalent bonds is possible but for the neutral system may be impeded by the presence of activation energy barriers to insertion.

Acknowledgment. D.S.Y. thanks the National Science Foundation and the donors of the Petroleum Research Fund, administrated by the American Chemical Society, for support of this research. D.B.P. thanks Steve Mitchell for the insightful, stimulating conversations.

References and Notes

(1) Gale, P. A. *Philos. Trans. R. Soc. London A* **2000**, *358*, 431.
(2) Siegbahn, P. E. M.; Blomberg, M. R. A. *Chem. Rev.* **2000**, *100*, 421.
(3) Malmstrom, B. G.; Wittung-Stafshede, P. *Coord. Chem. Rev.* **1999**, *185−186*, 127.
(4) Cacciapaglia, R.; Mandolini, L. *Chem. Soc. Rev.* **1993**, *22*, 221.
(5) Cacciapaglia, R.; DiStefano, S.; Kelderman, E.; Mandolini, L. *Angew. Chem., Int. Ed. Engl.* **1999**, *38*, 348.
(6) Hill, S. E.; Glendening, E. D.; Feller, D. *J. Phys. Chem. A* **1997**, *101*, 6125.
(7) Bauschlicher, C. W. J.; Langhoff, S. R.; Partridge, H.; Rice, J.; Komornicki, A. *J. Chem. Phys.* **1991**, *95*, 5142.
(8) Parnis, J. M.; Mitchell, S. A.; Rayner, D. M.; Hackett, P. A. *J. Phys. Chem.* **1988**, *92*, 3869.
(9) Fangstrom, T.; Kirrander, A.; Eriksson, L. A.; Lunnell, S. *J. Chem. Soc., Faraday Trans.* **1998**, *94*, 777.
(10) Alvarez, E. J.; Wu, H. F.; Liou, C. C.; Brodbelt, J. *J. Am. Chem. Soc.* **1996**, *118*, 9131.
(11) Zagorevkii, D. V.; Holmes, J. L.; Watson, C. H.; Eyler, J. R. *Eur. Mass Spectrom.* **1997**, *3*, 27.
(12) Huang, S. K.; Allison, J. *Organometallics* **1983**, *2*, 883.
(13) Burnier, R. C.; Byrd, G. D.; Freiser, B. S. *J. Am. Chem. Soc.* **1981**, *103*, 4360.
(14) More, M. B.; Ray, D.; Armentrout, P. B. *J. Phys. Chem. A* **1997**, *101*, 831.
(15) More, M. B.; Ray, D.; Armentrout, P. B. *J. Phys. Chem. A* **1997**, *101*, 7007.
(16) Weisshaar, J. C. *Acc. Chem. Res.* **1993**, *26*, 213.
(17) Parnis, J. M.; Mitchell, S. A.; Hackett, P. A. *J. Phys. Chem.* **1990**, *94*, 8152.
(18) Yang, D. S.; Hackett, P. A. *J. Electron Spectrosc. Relat. Phenom.* **2000**, *106*, 153.
(19) Berces, A.; Zgierski, M. Z.; Yang, D. S. In *Computational Molecular Spectroscpy*; Jensen, P., Bunker, P. R., Eds.; John Wiley & Sons: Sussex, 2000.
(20) Dietz, T. G.; Powers, D. E.; Duncan, M. A.; Smalley, R. E. *J. Chem. Phys.* **1981**, *74*, 6511.
(21) Willey, W. C.; McLaren, I. H. *Rev. Sci. Instrum.* **1955**, *26*, 1150.
(22) Pedersen, D. B.; Parnis, J. M.; Rayner, D. M. *J. Chem. Phys.* **1998**, *109*, 551.
(23) Mitchell, S. A.; Lian, L.; Rayner, D. M.; Hackett, P. A. *J. Chem. Phys.* **1995**, *103*, 5539.
(24) Lian, L. Mitchell, S. A.; Rayner, D. M. *J. Chem. Phys.* **1994**, *98*, 11637.
(25) Becke, A. D. *J. Chem. Phys.* **1993**, *98*, 5648.
(26) Perdew, J. P. *Phys. Rev. B* **1986**, *33*, 8822.
(27) Hay, P. J.; Wadt, W. R. *J. Chem. Phys.* **1985**, *82*, 270.
(28) Frisch, M. J.; Trucks, G. W.; Schlegel, H. B.; Gill, P. M. W.; Johnson, B. G.; Robb, M. A.; Cheeseman, J. R.; Keith, T.; Petersson, G. A.; Montgomery, J. A.; Raghavachari, K.; Al-Laham, M. A.; Zakrzewski, V. G.; Ortiz, J. V.; Foresman, J. B.; Cioslowski, J.; Stefanov, B. B.; Nanayakkara, A.; Challacombe, M.; Peng, C. Y.; Ayala, P. Y.; Chen, W.; Wong, M. W.; Andres, J. L.; Replogle, E. S.; Gomperts, R.; Martin, R. L.; Fox, D. J.; Binkley, J. S.; Defrees, D. J.; Baker, J.; Stewart, J. P.; Head-Gordon, M.; Gonzalez, C.; Pople, J. A. *Gaussian 94*, revision D.4; Gaussian, Inc.: Pittsburgh, PA, 1995.
(29) Steinfeld, J. I.; Francisco, J. S.; Hase, W. I. *Chemical Kinetics and Dynamics;* Prentice Hall: New York, 1989.
(30) Lian, L.; Hackett, P. A.; Rayner, D. M. *J. Chem. Phys.* **1993**, *99*, 2583.
(31) Wen, Y.; Porembski, M.; Ferrett, T. A.; Weisshaar, J. C. *J. Phys. Chem. A* **1998**, *102*, 8362.
(32) Gilbert, R. G.; Smith, S. C. *Theory of unimolecular and recombination reactions;* Blackwell Scientific Publications: Oxford and Cambridge MA, 1990.
(33) Moore, C. E. *Atomic Energy Levels, v2;* National Bureau of Standards, 1952.
(34) Raghquadiari, K.; Pople, J. A. *Int. J. Quantum Chem.* **1981**, *20*, 167.
(35) Godbout, N.; Salahub, D. R.; Audzelui, J.; Wimmer, E. *Can. J. Chem.* **1992**, *70*, 560.
(36) Herzberg, G. H. *Molecular Spectra and Molecular Structure II, Electronic Structure of Polyatomic Molecules;* Krieger: Malabar, Florida, 1989.
(37) Balasubramanian, K. *J. Chem. Phys.* **1988**, *89*, 5731.
(38) Matsunaga, N.; Koseki, S.; Gordon, M. S. *J. Chem. Phys.* **1996**, *104*, 7988.
(39) Willis, P. A.; Stauffer, H. U.; Hinrichs, R. Z.; Davis, H. F. *J. Phys. Chem. A.* **1999**, *103*, 3706.
(40) Chatt, J.; Duncanson, L. A. *J. Chem. Soc.* **1953**, 2939.
(41) Dewar, M. J. S. *Bull. Soc. Chim. Fr.* **1951**, 79.
(42) Alvanipour, A.; Atwood, J. L.; Bott, S. G.; Junk, P. C.; Kynast, U. H.; Prinz, H. *J. Chem. Soc., Dalton Trans.* **1998**, 1223.
(43) Beaton, S. A.; Gerry, M. C. L. *J. Chem. Phys.* **1999**, *110*, 10715.
(44) Mitchell, S. A. In *Gas-Phase Metal Reactions;* ACS Symposium Series; Elsevier: Amsterdam, 1992.
(45) Blomberg, M.; Brandemark, U.; Siegbahn, P. *J. Am. Chem. Soc.* **1983**, *105*, 5557.
(46) Blomberg, M. R. A.; Siegbahn, P. E. M.; Svensson, M. *J. Phys. Chem.* **1991**, *95*, 4313.
(47) Armentrout, P. B. *Acc. Chem. Res.* **1989**, *22*, 315.